# Angular dependence of electron emission induced by grazing-ion–surface collisions

M. S. Gravielle,[1] J. E. Miraglia,[1] G. G. Otero,[2] E. A. Sánchez,[2] and O. Grizzi[2]
[1]*Instituto de Astronomía y Física del Espacio (IAFE ), Consejo Nacional de Investigaciones Científicas y Técnicas, Casilla de Correo 67, Sucursal 28, 1428 Buenos Aires, Argentina and Departamento de Física, FCEN, Universidad de Buenos Aires, 1428 Buenos Aires, Argentina*
[2]*Centro Atómico Bariloche and Instituto Balseiro, Comisión Nacional de Energía Atómica and Consejo Nacional de Investigaciones Científicas y Técnicas, 8400 San Carlos de Bariloche, Río Negro, Argentina*
(Received 17 June 2003; published 21 April 2004)

In this work, electron emission spectra produced by impact of fast protons on Al(111) surfaces are theoretically and experimentally studied. Contributions coming from the different electronic sources of the metal—atomic inner shells and valence band—are analyzed as a function of the angle of electron emission. In the forward direction, the inner-shell ionization process is the dominant mechanism. The valence emission, instead, becomes important when the ejection angle is separated from the specular-reflection direction. In both angular regions, theoretical and experimental values are in reasonable agreement. The energy shift and broadening of the convoy electron peak at glancing observation angles are well described by the present model, which takes into account the influence of the induced surface field on the ionized electron.

DOI: 10.1103/PhysRevA.69.042902 PACS number(s): 34.50.Dy, 34.50.Bw

## I. INTRODUCTION

Electron emission produced during the grazing scattering of fast ions from solid surfaces has been extensively investigated during the last several years [1–12]. The interest in these collisions has been motivated by the particular features of the collisional system, which allow one to extract specific information about the electronic structure of the surface from the electron spectra.

When a fast ion collides on a metal surface with an incidence angle smaller than a given critical angle, the ion is specularly reflected from the surface without penetrating inside the bulk. At high impact velocities, the charge state of the ion can be considered as fixed [14,15], and the projectile moving along a grazing trajectory induces the emission of electrons from the metal. These electrons may come from two different electronic sources: the valence band and the inner shells of target atoms.

With the purpose of analyzing the angular regions where inner-shell and valence ionization processes are relevant, we study both theoretically and experimentally the electron distributions produced by fast protons impinging grazingly on an Al(111) surface. We consider different angles of electron ejection, varying not only the elevation angle relative to the surface but also the angle between the direction of emission and the scattering plane.

In the present work, inner-shell and valence contributions are calculated separately. To evaluate the inner-shell emission yield, also called core contribution, we employ the recently proposed *field distorted-wave* (FDW) approximation [16]. It is an extension of the continuum-distorted-wave–eikonal-initial-state (CDW-EIS) approximation, which allows us to describe the ionization from atomic bound states, taking into account the effect of the electric field induced by the projectile. In the model, atomic ionization probabilities depend not only on the modulus of the impact parameter, but also on its direction. The contribution from the valence band is calculated within the binary collisional formalism, using the *modified specular reflection* (MSR) model to represent the surface wake interaction [17]. The plasmon decay mechanism is not included in the valence emission because it only contributes in the low electron-energy range [18–20], which is not considered here.

The article is organized as follows. In Sec. II the theoretical models used to calculate inner-shell and valence contributions are outlined. The experimental technique is described in Sec. III. In Sec. IV results are shown and discussed, and Sec. V contains our conclusions.

## II. THEORETICAL MODEL

We consider a heavy projectile ($P$), of charge $Z_P$ and mass $M_P$, impinging grazingly on a metal surface. As a result of the collision, an electron ($e$) belonging to the solid is emitted with momentum $\vec{k}_f$, which is measured in vacuum semispace. Due to the large mass $M_P$ of the projectile, the description of its motion in terms of a classical trajectory is a reasonable approximation. We use a frame of reference fixed to the position of the first atomic layer, with the projectile trajectory contained in the $x-z$ plane, and the surface in the $x-y$ plane (see Fig. 1). Within this frame, the position of the projectile at a given time $t$ reads $\vec{R}(x)=(x,0,Z(x))$, with $Z(x)$ the classical projectile trajectory. Atomic units are used unless otherwise stated.

For grazing incidence, the projectile path can be divided into differential portions, with width $\Delta x$, situated at different distances $Z(x)$ from the surface. In every portion, the component of the projectile velocity perpendicular to the surface is considered negligible, and the ion moving parallel to the surface plane with velocity $\vec{v}_s=(v_s,0,0)$ ionizes electrons from the solid. In the case of metal surfaces, emitted electrons can be separated into inner-shell and valence-band electrons, according to their initial binding energies. The differential probability of electron emission, $dP/d\vec{k}_f$, is ob-

 

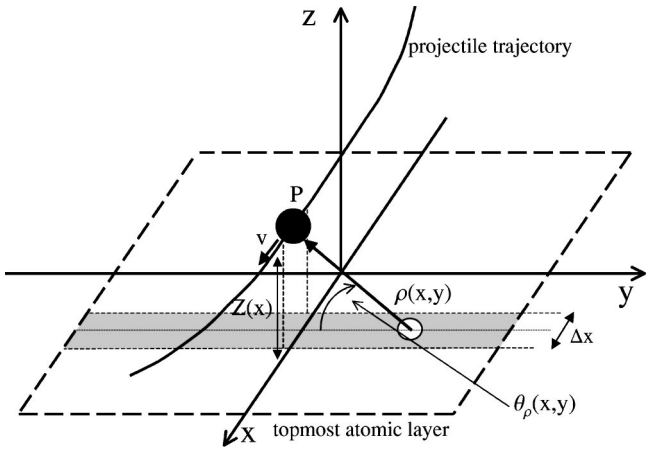


FIG. 1. Schematic picture of the coordinate system.

tained by adding the core and valence contributions along the projectile trajectory; that is,

$$\frac{dP}{d\vec{k}_f} = \int_{-\infty}^{+\infty} dx\ (P_{\vec{k}_f}^{(\mathrm{is})}(x) + P_{\vec{k}_f}^{(\mathrm{val})}(x)), \tag{1}$$

where $P_{\vec{k}_f}^{(j)}(x)$, $j=(\mathrm{is},\mathrm{val})$ denotes the transition probability per unit path to the final state with momentum $\vec{k}_f$ from inner-shell (is) and valence-band (val) states, respectively. The theoretical models employed to evaluate the emission probabilities $P_{\vec{k}_f}^{(\mathrm{is})}$ and $P_{\vec{k}_f}^{(\mathrm{val})}$ in this work will be summed up in the following sections.

The double-differential yield of electron emission $d^2P/d\varepsilon_f d\Omega_f$ is derived from Eq. (1) as $d^2P/d\varepsilon_f d\Omega_f = k_f dP/d\vec{k}_f$, where $\varepsilon_f = k_f^2/2$ is the electron energy and $\Omega_f = (\theta_e, \phi_e)$ is the ejection angle. The angle $\theta_e$ is the elevation angle with respect to the surface and $\phi_e$ is the angle between the direction of emission and the scattering plane, measured on the surface plane. In this way, the final electron momentum, outside the solid, reads $\vec{k}_f = k_f(\cos\theta_e \cos\phi_e, \cos\theta_e \sin\phi_e, \sin\theta_e)$.

### A. Inner-shell emission

Since core electrons are strongly localized around the target nucleus, when the projectile moves along the portion $\Delta x$ of its trajectory, it ionizes essentially electrons bounded to atoms situated at the first atomic plane of the corresponding surface band (see Fig. 1). Under this assumption, the probability per unit path $P_{i\vec{k}_f}^{(is)}(x)$, for the transition from the initial bound state $i$ to the final state $f$ with momentum $\vec{k}_f$, is given by

$$P_{i\vec{k}_f}^{(is)}(x) = \delta_S \int_{-\infty}^{+\infty} dy\ \mathcal{P}_{i\vec{k}_f}^{(at)}(\vec{\rho}(x,y)), \tag{2}$$

where $\mathcal{P}_{i\vec{k}_f}^{(at)}(\vec{\rho})$ is the probability of atomic ionization depending on the impact parameter $\vec{\rho}$, and $\delta_S$ is the surface atomic density, which is considered as constant. In Eq. (2) the impact parameter depends on the position of the surface atom considered, being

$$\rho(x,y) = \sqrt{y^2 + Z^2(x)}, \quad \theta_\rho(x,y) = \arctan\left(\frac{Z(x)}{-y}\right) \tag{3}$$

the modulus and the azimuthal angle, respectively, of $\vec{\rho}(x,y)$.

In collisions with metal surfaces, the atomic ionization is developed in the presence of the induced potential $V_0$ originated by the surface. To describe this process we employ the FDW approximation, which is a distorted wave theory that takes into account the action of the wake potential on the ejected electron. Here we resume the main results of the FDW model, while details of its derivation can be found in Ref. [16].

Within FDW formalism, the interaction of the electron with the surface induced field, $\vec{E}_0(\vec{r},t) = -\vec{\nabla}_{\vec{r}} V_0(\vec{r},t)$, is included in the initial $\phi_i^+$ and final $\phi_f^-$ collisional states by means of the Volkov ansatz [21]. The distorted wave functions are defined from $\phi_i^+$ and $\phi_f^-$ by introducing the Coulomb distortions of the projectile and the target

$$\chi_i^+(\vec{r}_T,t) = \phi_i^+(\vec{r}_T,t) E_P^+(-\vec{v}_s,\vec{r}_P),$$

$$\chi_f^-(\vec{r}_T,t) = \phi_f^-(\vec{r}_T,t) D_T^-(\vec{k}_T,\vec{r}_T) D_P^-(\vec{k}_P,\vec{r}_P), \tag{4}$$

where $\vec{r}_P$ and $\vec{r}_T$ are the position vectors of $e$ with respect to the projectile $P$ and to the target nucleus $T$ of charge $Z_T$, respectively. The vectors

$$\vec{k}_T = \vec{k}_f + \vec{A}_f(t),$$

$$\vec{k}_P = \vec{k}_f - \vec{v}_s + \vec{A}_f(t), \tag{5}$$

are the electron momenta with respect to $T$ and $P$, respectively, involved in the hard atomic collision, with $\vec{k}_f$ the final electron momentum measured by the detector, after being accelerated by the field $\vec{E}_0$. The vector $\vec{A}_f(t)$ is the vector potential of the surface field $\vec{E}_0$ acting on the ionized electron,

$$\vec{A}_f(t) = \vec{A}_{f0} - \int_{+\infty}^{t} dt' \vec{E}_0(\vec{R}(t'),t'), \tag{6}$$

where $\vec{R}(t)$ denotes the projectile position at the time $t$ and $\vec{A}_{f0}$ is a constant value. In Eq. (4), $D_c^{\pm}(\vec{k},\vec{r}) = F_c^{\pm}(k)\,{}_1F(\pm iZ_c/k, 1, \pm ikr - i\vec{k}\cdot\vec{r})$ represents the Coulomb distortion produced by the charge $Z_c$, and $E_c^{\pm}(\vec{k},\vec{r}) = \exp[\mp iZ_c/k\ \ln(kr \mp \vec{k}\cdot\vec{r})]$ is the eikonal phase, with $c = P,T$. In the definition of $D_c^{\pm}$, the function ${}_1F_1$ denotes the confluent hypergeometric function, $k = |\vec{k}|$, and

$$F_c^{\pm}(k) = \exp\left(\frac{\pi Z_c}{2k}\right)\Gamma(1 \mp iZ_c/k), \quad c = P,T, \tag{7}$$

is a normalization factor that coincides with the value of the Coulomb wave function at $\vec{r} = \vec{0}$ (Jost function).

The FDW transition matrix, $\mathcal{T}_{i\vec{k}_f}^{\mathrm{FDW}}$, is derived from $\chi_i^+$ and $\chi_f^-$ as the first order of a distorted wave theory. After lengthy algebra, $\mathcal{T}_{i\vec{k}_f}^{\mathrm{FDW}}$ can be expressed in terms analytical Nordsieck integrals, and an approximated expression of it is given by [16]

$$\mathcal{T}_{i\vec{k}_f}^{\mathrm{FDW}} \simeq \frac{F_P^{(s)-*}(k_P)}{F_P^{-*}(|\vec{k}_f-\vec{v}_s|)}\frac{F_T^{-*}(k_T)}{F_T^{-*}(k_f)}\mathcal{T}_{i\vec{k}_f}^{\mathrm{CDW\text{-}EIS}}, \tag{8}$$

where $\mathcal{T}_{i\vec{k}_f}^{\mathrm{CDW\text{-}EIS}}$ is $T$-matrix element calculated with the usual CDW-EIS approximation [22]. Note that $T_{i\vec{k}_f}^{\mathrm{CDW\text{-}EIS}}$ can be obtained from the distorted wave functions defined in Eq. (4) by fixing $\vec{E}_0=\vec{0}$. The function $F_P^{(s)-}$ takes into account that in collisions with metals the projectile is shielded by valence electrons, and the $P$-$e$ interaction is not more represented by a Coulomb potential. $F_P^{(s)-}(k)$ is defined as the value at the origin of the eigenfunction with momentum $\vec{k}$ corresponding to the screening potential $V_P^{(s)}=-Z_P\exp(-\lambda r_P)/r_P$, with $\lambda=w_s(v_s^2+v_F^2/3)^{-1/2}$, which describes the dynamic shielding of the projectile. The parameter $w_s$ denotes the surface plasmon frequency and $v_F$ is the Fermi velocity.

In Eq. (8), the electron momenta $\vec{k}_T$ and $\vec{k}_P$ are expressed as a function of the $x$ position of the ion,

$$\vec{k}_T=\vec{k}_f+\vec{A}_f(x),$$

$$\vec{k}_P=\vec{k}_f-\vec{v}_s+\vec{A}_f(x), \tag{9}$$

where the vector potential

$$\vec{A}_f(x)=-\vec{E}_0(\vec{R}(x),x/v_s)t_{int} \tag{10}$$

has been derived from Eq. (6) by considering that: (i) the time dependence of $\vec{E}_0$ is determined by the projectile position $\vec{R}(x)$, with $x=v_st$, and (ii) the field $\vec{E}_0=(E_{0x},0,E_{0z})$ does not vary appreciably along an effective interaction time $t_{int}$ when the interaction takes place. Therefore, the action of the surface field on the emitted electron produces a supplementary momentum transfer $\vec{A}_f(x)$, which depends on the point of the projectile trajectory considered.

The field $\vec{E}_0$ acting on the emitted electron can be expressed as the sum of the fields $\vec{E}_0^{(P)}$ and $\vec{E}_0^{(e)}$, which are induced by the projectile and the ejected electron, respectively. The medium cannot immediately react to the presence of the electron, and the field $\vec{E}_0^{(e)}$ arises around a time $t_{wf}$ after the hard atomic collision took place. The time $t_{wf}$ is associated with the so-called wake formation time [23,24]. Taking into account that emitted electrons are mainly produced inside the solid, we have roughly defined $\vec{E}_0^{(e)}$ as a step function, $\vec{E}_0^{(e)}(\vec{r},t)=\vec{E}_0^{(e)}\Theta(t-t_{wf})$, with $t_{wf}\approx\pi/(4\,w_p)$ and $w_p$ the bulk plasmon frequency. The field induced by projectile $\vec{E}_0^{(P)}$ has been derived by employing the specular-reflection (SR) model [23,25], while the field induced by the electron $\vec{E}_0^{(e)}$ has been obtained from the stopping of electrons inside metals [26].

The *effective* interaction time $t_{int}$, used in Eq. (10), is defined as the interval of time in which the electric field $\vec{E}_0$ is important. For the collisional system composed by 100 keV $H^+$ impinging on aluminum, considered in the present work, we estimate the interaction time as $t_{int}\approx t_{wf}$. Then, in the range $[0,t_{int}]$ the contribution of $\vec{E}_0^{(e)}$ in Eq. (10) can be neglected, the electron being mainly accelerated by the field $\vec{E}_0^{(P)}$ during the collisional time. Around $t\approx t_{int}$ the projectile has already separated approximately 3–4 a.u. from the nucleus target. Subsequently, the ionized electron suffers the simultaneous action of the opposite fields $\vec{E}_0^{(P)}$ and $\vec{E}_0^{(e)}$, whose absolute values are nearly similar for intermediate electron energies. So, for $t>t_{int}$ the electron keeps escaping from the projectile with a nearly constant velocity. Therefore, under this picture convoy electrons, which are primary produced at the closest distance to the surface, abandon the medium with a velocity larger than the projectile one, moving far away from the incident ion. By the time when the projectile crosses the surface (jellium border), the convoy electron is separated a distance of several ten atomic units from the projectile. For other collisional systems, the definition of $t_{int}$ should be opened to discussion.

Finally, the atomic ionization probability $\mathcal{P}_{i\vec{k}_f}^{(at)}(\vec{\rho})=|\mathcal{A}_{i\vec{k}_f}^{(at)}(\vec{\rho})|^2$ is derived from Eq. (8) by using the eikonal transformation [27]

$$\mathcal{A}_{i\vec{k}_f}^{(at)}(\vec{\rho})=\frac{2\pi}{v_s}\int d\vec{\eta}\exp(i\,\vec{\eta}\cdot\vec{\rho})\mathcal{T}_{i\vec{k}_f}^{\mathrm{FDW}}, \tag{11}$$

where $\vec{\eta}$ is the component of the transferred momentum perpendicular to $\vec{v}_s$. The inner-shell emission probability per unit path, $P_{\vec{k}_f}^{(is)}(x)$, is obtained from Eq. (2) by adding over all occupied initial states; that is,

$$P_{\vec{k}_f}^{(is)}(x)=\sum_i P_{i\vec{k}_f}^{(is)}(x). \tag{12}$$

In the calculations, the atomic bound states have been described by Hartree-Fock double-$z$ functions [28], and an effective charge satisfying the binding energy has been used to represent the final continuum state around the target. The factor $F_P^{(s)-}$ has been numerically evaluated by using the code of Ref. [29].

### B. Valence emission

To evaluate the electron emission from the valence band of the solid we employ the binary collisional theory [30]. This formalism describes the multiple collisions of the projectile with valence electrons, which form the free-electron gas, along its trajectory.

Within the binary collisional formalism, the probability per unit path $P_{\vec{k}_i\vec{k}_f}^{(val)}(x)$, for the transition from the initial

valence-band state with momentum $\vec{k}_i'$ to the final state with momentum $\vec{k}_f'$, reads [30]

$$P^{(val)}_{\vec{k}_i'\vec{k}_f'}(x) = \frac{2\pi}{v_s}\delta(\Delta)|\mathcal{T}_{\vec{k}_i'\vec{k}_f'}|^2, \quad (13)$$

where $\mathcal{T}_{\vec{k}_i'\vec{k}_f'}$ is the $T$-matrix element corresponding to the inelastic transition $\vec{k}_i' \rightarrow \vec{k}_f'$, and the prime indicates that the initial and final electron momenta are both measured inside the solid. The delta function imposes the energy conservation, $\Delta = \vec{v}_s \cdot (\vec{k}_f' - \vec{k}_i') - (\varepsilon_{\vec{k}_f'} - \varepsilon_{\vec{k}_i'})$, with $\varepsilon_{\vec{k}_i'}(\varepsilon_{\vec{k}_f'})$ the initial (final) electron energy. In the first Born approximation, the transition matrix reads $T^B_{\vec{k}_i'\vec{k}_f'} = \langle \phi^-_{\vec{k}_f'} | V_{Pe} | \phi^+_{\vec{k}_i'} \rangle$, where $V_{Pe}$ is the Coulomb $P$-$e$ interaction shielded by the presence of the other valence electrons, and $\phi^+_{\vec{k}_i'}$ and $\phi^-_{\vec{k}_f'}$ are the initial and final electronic states, respectively.

We use the surface jellium model to represent the conduction band of the solid. In this model, the electrons are confined inside the solid by a square barrier, which is placed at a distance $D/2$ in front of the first atomic layer, with $D$ the interplanar separation. By using the jellium model, the $T$-matrix element $\mathcal{T}^B_{\vec{k}_i'\vec{k}_f'}$ is expressed as an integral in the momentum space

$$\mathcal{T}^B_{\vec{k}_i'\vec{k}_f'} = \frac{Z_P}{2\pi^2}\int_{-\infty}^{+\infty} du \frac{W_{Pe}(u) f(u)}{(p_s^2 + u^2)}, \quad (14)$$

where $W_{Pe}(u)$ is a screening factor, which depends on the approximation used to represent the induced potential, and $\vec{p} = \vec{k}_f' - \vec{k}_i' = (\vec{p}_s, p_z)$ is the transferred electron momentum, with $\vec{p}_s$ the component of $\vec{p}$ parallel to the surface. The factor $f(u)$ represents an one-dimensional electronic form factor, whose expression can be found in Ref. [30]. (Also, see Ref. [17] for details.)

To evaluate $W_{Pe}$ we employ the MSR model, which is derived from the specular reflection model [23] by including the momentum transfer perpendicular to the surface, $p_z$, in the wake potential. Such a modification corrects the failure found in the binary results when SR model is used [31]. The MSR screening factor reads [17]

$$W^{(MSR)}_{Pe}(u) = V^{(+)}(u)\Theta(Z') - \frac{1}{\epsilon}V^{(-)}(u)\Theta(-Z'), \quad (15)$$

with

$$V^{(\pm)}(u) = \frac{(1-\epsilon)}{(1+\epsilon)}\exp(-p_s|Z'|) \pm \exp(-iuZ'), \quad (16)$$

where $\epsilon = \epsilon(\vec{p}, \omega)$ is the bulk dielectric function, evaluated on the *total* momentum $\vec{p}$ and on the frequency $\omega = \vec{p}.\vec{v}_s$, and $Z' = Z(x) - D/2$ is the distance of the projectile to the jellium border. In the calculations, the bulk dielectric function $\epsilon(\vec{q}, \omega)$ is derived from the random-phase approximation (Lindhard's dielectric function) [32] together with the Mermin's prescription, which allows us to deal with finite values of the lifetime $1/\gamma$ [33].

The differential probability of valence-electron emission per unit path $P^{(val)}_{\vec{k}_f}(x)$ can be obtained from Eq. (13) by integrating on the all initial valence-band states,

$$P^{(val)}_{\vec{k}_f}(x) = (k_{fz}/k_{fz}') \int d\vec{k}_i' \ \rho_e \ \Theta(v_F - k_i') P^{(val)}_{\vec{k}_i'\vec{k}_f'}(x), \quad (17)$$

where the unitary Heaviside function $\Theta(v_F - k_i')$ restricts the initial states to those contained inside the Fermi sphere, with $v_F$ the Fermi velocity, and $\rho_e = 2$ takes into account the spin states. In the derivation of Eq. (17), we have replaced the momentum $\vec{k}_f'$ measured inside the solid by the momentum $\vec{k}_f = (\vec{k}_{fs}, k_{fz})$ measured outside the solid, in the vacuum region, by using the relations $\vec{k}_{fs} = \vec{k}_{fs}'$ and $k_{fz} = (k_{fz}'^2 - k_c^2)^{1/2}$, with $k_c = (2E_W + v_F^2)^{1/2}$ and $E_W$ the work function.

## III. EXPERIMENTAL DETAILS

The experiments were conducted in an ultrahigh vacuum chamber at an operating pressure of $3 \times 10^{-10}$ Torr with the ion beam line open. The ions were generated in a radio frequency source, mass selected and collimated to better than 0.1°. The emitted electrons were analyzed with a custom-made [34] cylindrical mirror energy spectrometer working at 1% energy resolution and ±0.7° angular resolution. The rotation of the inner cylinder around its main axis defines the electron observation angles $\theta_e$ and $\phi_e$, measured with respect to the surface and the scattering planes, respectively. These angles cannot be chosen independently; for grazing observation ($\theta_e < 10°$), the azimuthal angle $\phi_e$ remains in the scattering plane ($\phi_e \leqslant 1°$), but for large elevation angles ($\theta_e \geqslant 20°$) $\phi_e$ moves away from it [35]. For the present measurements the incident direction was selected to be random, i.e., not along a low-index surface crystallographic axis. All the electron energy spectra shown here have been corrected for the transmission function of the spectrometer in order to compare them with the calculated electron distributions.

The Al(111) sample was prepared by repeated cycles of grazing sputtering (0.5°–2° incidence angle) with 20 keV $Ar^+$ followed by annealing at 450 °C. The azimuthal orientation of the surface was continuously changed during the Ar irradiation. This method produces a very flat surface as has been shown in previous works [11,37]. The surface roughness was checked *in situ* by measuring the convoy electron emission produced by 60 keV $H^+$ at 1° incidence and the Al Auger electron peak produced by 20 keV $Ne^+$ as a function of the incident angle. Both measurements show that the vast majority of the incident ions (>90%) interact with flat surface regions [10,36]. The surface cleanliness, achieved with the repeated sputtering-annealing cycles, was verified with Auger electron spectroscopy before and after performing the measurements.

## IV. RESULTS

Our study has concentrated on 100 keV protons impinging on an Al(111) surface with the angle of incidence $\theta_i = 1°$. As the Al atoms contain three electrons in the outermost

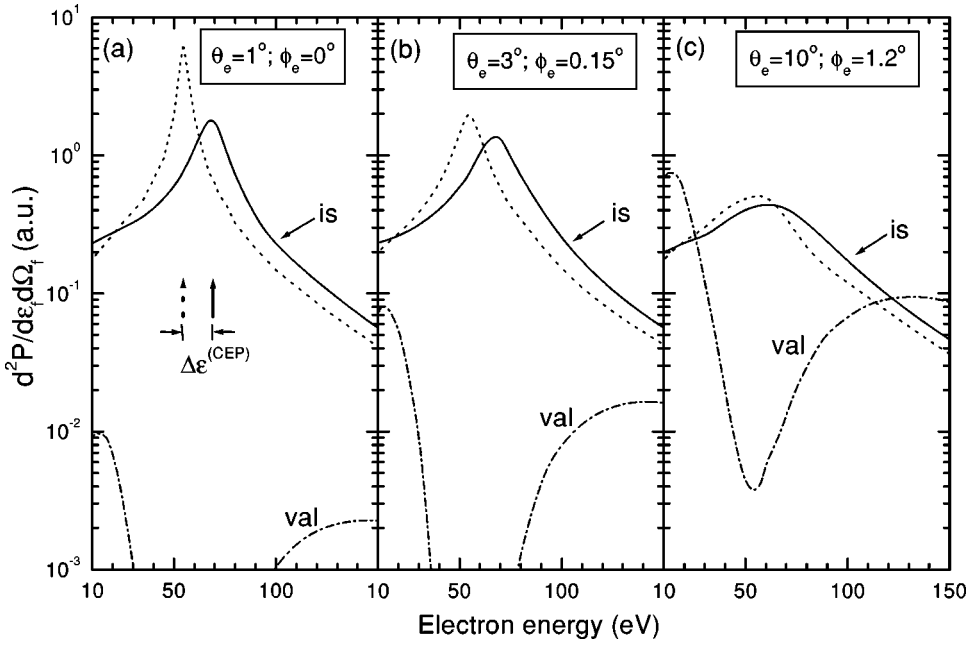


FIG. 2. Inner-shell and valence-band emission probabilities, as a function of the electron energy, for 100 keV protons impinging on an Al(111) surface with the incidence angle $\theta_i=1°$. Three different electron ejection angles are considered: (a) $\Omega_f=(\theta_e=1°,\phi_e=0°)$, (b) $(\theta_e=3°,\phi_e=0.15°)$, and (c) $(\theta_e=10°,\phi_e=1.2°)$. Solid line, inner-shell emission probability calculated with the FDW approximation; dashed-dotted line, valence emission probability obtained with the binary MSR model; dotted line, inner-shell emission probability evaluated with the CDW-EIS approximation, in absence of the surface interaction. The symbol $\Delta\varepsilon^{(CEP)}$ denotes the energy shift of the CEP, with respect to its position for $\vec{E}_0=\vec{0}$.

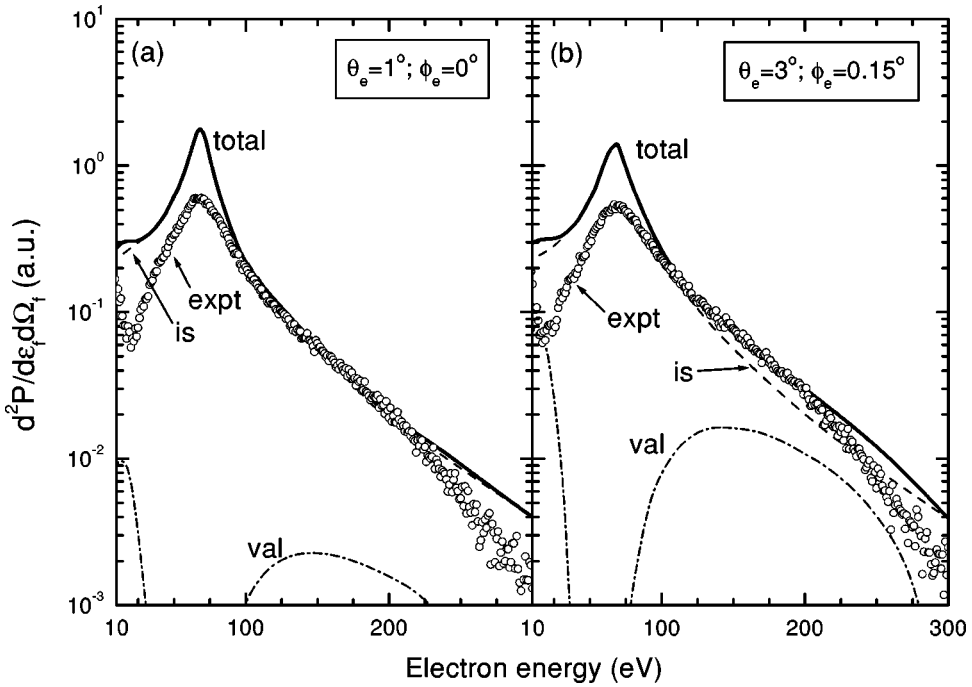


FIG. 3. Double differential probability of electron emission, $d^2P/d\varepsilon_f d\Omega_f$, for 100 keV-protons impinging on an Al(111) surface with the incidence angle $\theta_i=1°$. Two electron observation angles around the forward direction are considered: (a) $\Omega_f=(\theta_e=1°,\phi_e=0°)$ and (b) $(\theta_e=3°,\phi_e=0.15°)$. Empty circles, present experimental values, normalized with the theory. Theoretical predictions: solid line, total probability of electron emission calculated by adding inner-shell (with the FDW model) and binary valence contributions; dashed and dashed-dotted lines, inner-shell and valence emission probabilities, respectively.

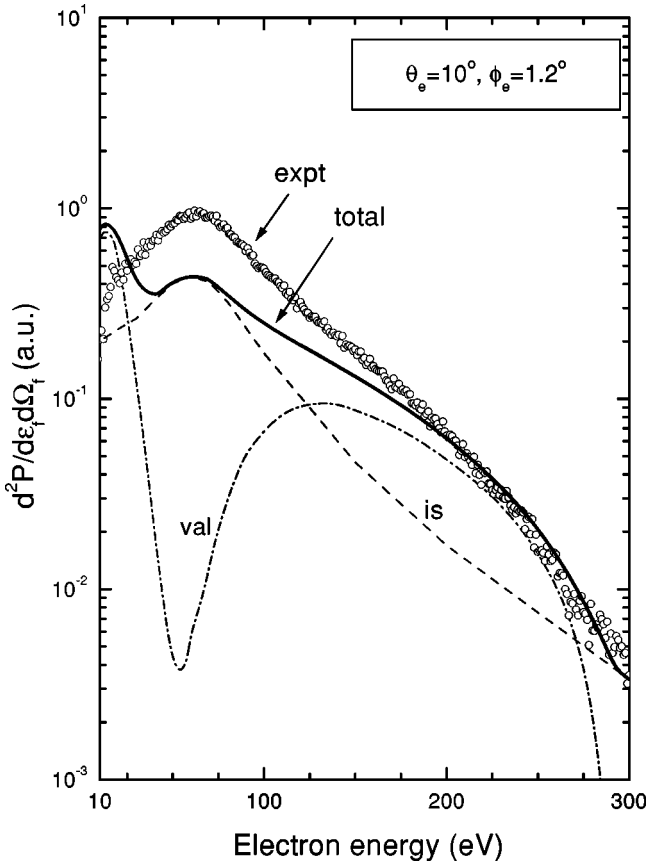


FIG. 4. Similar to Fig. 3 for the electron observation angle $\Omega_f = (\theta_e = 10°, \phi_e = 1.2°)$.

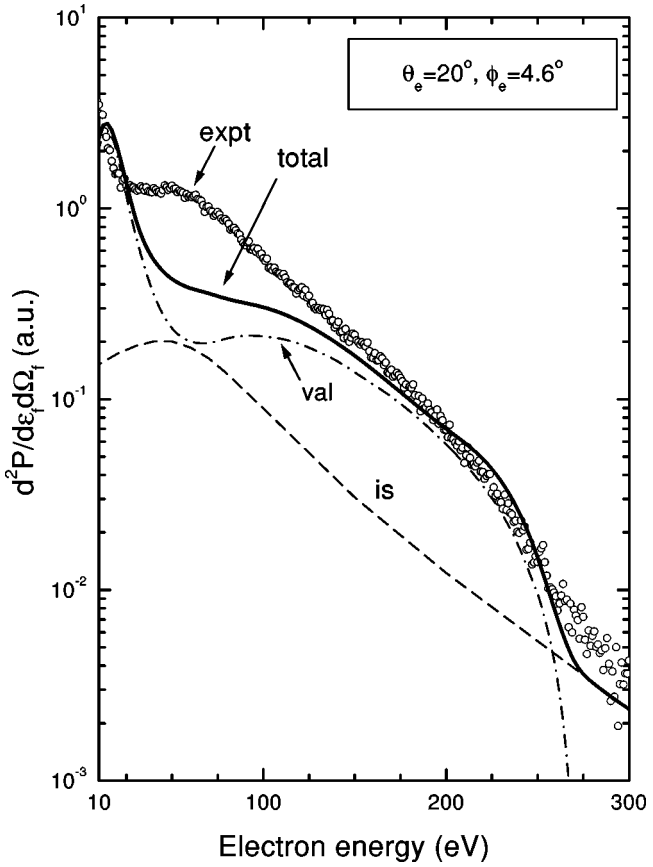


FIG. 5. Similar to Fig. 3 for the electron observation angle $\Omega_f = (\theta_e = 20°, \phi_e = 4.6°)$.

shell $n=3$, we consider that they cede these external electrons to the free-electron gas, keeping the rest of the electrons in the inner shells. The parameters used to describe the aluminum surface are: the Fermi velocity $v_F = 0.91$ a.u., the interplanar distance $D = 4.4$ a.u., the work function $E_W = 0.15$ a.u., and the damping coefficient $\gamma = 0.037$ a.u. [37].

In the calculation of the core emission, only the initial states corresponding to the $L$ shell of aluminum were included in Eq. (12) because the $K$-shell ionization is negligible at the considered impact energy. For every initial state, the evaluation of $P^{(is)}_{i\vec{k}_f}$ involves a three-dimensional integration on the variables $\vec{\eta}$ and $y$ [Eqs. (11) and (2), respectively], that was numerically evaluated with a relative error lower than 3%. For the valence contribution, the numerical integration on $\vec{k}_i'$ [Eq. (17)] was done with a relative error of 1%. In both cases, the further integration on the variable $x$ involved in Eq. (1) was solved by interpolating approximately 20 pivots on the classical trajectory $Z(x)$, determined by the projectile-surface potential. To represent this interaction we employ the Molière potential [38] plus dynamical image potential given in Ref. [37]. Our theoretical probabilities were not convoluted with the acceptation angle of the detector.

Since our goal is to investigate the contribution originated from the different electronic sources of the metal, in Fig. 2 we compare calculated inner-shell and valence emission probabilities for three different angles of electron emission. We begin our analysis with the forward direction, moving the ejection angle around this angular region. At the angle $\Omega_f = (\theta_e = 1°, \phi_e = 0°)$, which coincides with the direction of the outgoing projectile, the core emission is more than one order of magnitude higher than the valence emission, even for the lowest electron energies where the valence contribution is maximal. For this particular ejection angle, the inner-shell emission probability displays a prominent structure, usually named convoy electron peak (CEP), which is associated with electrons that recede from the target atoms in close spacial correlation with the projectile [3]. Precisely, for electron energies around the CEP, the emission of valence electrons is *not* possible by binary collisions. It is due to the values of $\vec{k}_f$ reached by the binary ionization from the valence band are confined in the region [30]

$$K_{\min} \leqslant |\vec{k}_f - \vec{v}_s| \leqslant K_{\max}, \tag{18}$$

where $K_{\max} = [(v_s + v_F)^2 - k_c^2]^{1/2}$, and $K_{\min} = [(v_s - v_F)^2 - k_c^2]^{1/2} \Theta[v_s - (k_c + v_F)]$. It is a consequence of the energy conservation imposed by the delta function in Eq. (13). From Fig. 2, when the ejection angle $\Omega_f$ is separated from the forward direction, the valence contribution increases. For $\Omega_f = (\theta_e = 10°, \phi_e = 1.2°)$, the valence emission probability displays only a minimum around 54 eV, being higher than the inner-shell contribution for the lowest and the highest electron energies considered.

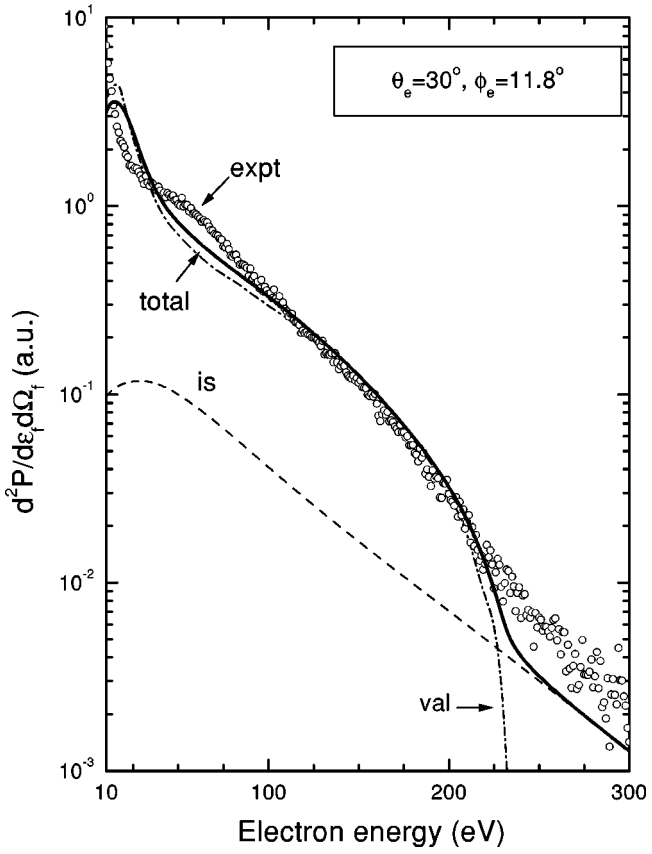


FIG. 6. Similar to Fig. 3 for the electron observation angle $\Omega_f = (\theta_e = 30°, \phi_e = 11.8°)$.

Since the position and shape of the CEP markedly depend on the surface interaction, to study the effect of the induced field on the core emission we also plot in Fig. 2 the probability of inner-shell ionization calculated with the usual CDW-EIS approximation, without taking into account either the surface field $\vec{E}_0$ or the shielding of the projectile. The core electron distribution obtained with the CDW-EIS theory shows a cusp-shaped peak placed at $\vec{k}_f \simeq \vec{v}_s$, similar to the one observed in collisions with gaseous targets. Within the FDW approximation, instead, the CEP is determined by the function $F_P^{(s)-}(k_P)$, which displays a wide maximum as $\vec{k}_P = \vec{k}_f - \vec{v}_s + \vec{A}_f(x) \to \vec{0}$. Then, in the presence of $\vec{E}_0$ the peak is moved to a new position $\vec{k}_f \simeq \vec{v}_s - \vec{A}_f(x)$, which is convoluted along the projectile path. For metals, the two components of the vector potential, $A_{fx}$ and $A_{fz}$, are negative in the whole $x$ range, and they originate an *acceleration* of the convoy electrons, shifting the position of the CEP to higher velocities, as indicated in Fig. 2(a). On the other hand, in the FDW theory the broadens of the CEP is produced by two different effects. First and mainly, the screening of the projectile inside the jellium, which is introduced in the model by replacing the Coulomb $P$-$e$ interaction by the screening potential $V_P^{(s)}$. And second and less important, the convolution of the momentum transfer $\vec{A}_f(x)$ along the projectile path $Z(x)$, which produces an additional smearing of the peak. As observed from Figs. 2(b) and 2(c), the surface interaction affects essentially electrons ejected in the forward direction, and this effect decreases rapidly when the elevation angle $\theta_e$ increases.

In Figs. 3–6, theoretical and experimental electron distributions corresponding to different ejection angles are plotted as a function of the final electron energy. Total predictions were obtained by adding valence and core emission probabilities, which were also included in the figures to display the electron energy range where each mechanism is dominant. In all the cases, the experimental spectra were normalized by using the theoretical values for the electron energy of 200 eV. Although this electron energy was arbitrarily chosen, the value of the normalization factor does not change appreciably for $\varepsilon_f$ varying in ±25 eV.

In Fig. 3, we analyze the forward electron emission. Around this direction, the most discernible structure of the theoretical and experimental spectra is the CEP, which is placed at an electron velocity $k_f > v_s$. For the two considered angles, $\theta_e = 1°$ and $\theta_e = 3°$, the theoretical curve presents a similar shape to the experimental one, displaying an energy shift of the CEP (with respect to its position for $\vec{E}_0 = \vec{0}$) $\Delta\varepsilon^{(CEP)} \simeq 13.5$ eV, which is close to the measured shift $\Delta\varepsilon_{\text{exp}}^{(CEP)} \simeq 14.5$ eV. Although for both observation angles the agreement found with the experiments is reasonable, it should be remarked that for $\theta_e = 1°$, ionized electrons travel a long distance through the jellium before being emitted to the vacuum, losing energy in multiple collisions along the outgoing path. This effect (transport) has not been included in our theoretical model, which only gives the *primary* electron distribution that is obtained by considering that electrons ionized from surface atoms are directly ejected to the vacuum. When the emission angle is slightly separated from the grazing direction, as for $\theta_e = 3°$, the path of ionized electrons inside the jellium decreases rapidly, and in this case, our theoretical results could be directly compared with the experimental data.

At the angle $\Omega_f = (\theta_e = 10°, \phi_e = 1.2°)$, displayed in Fig. 4, the valence emission becomes the dominant mechanism at low and high electron energies, in the velocity region usually known as *binary ridge*. In the electron momentum space, the binary sphere is determined from Eq. (18) by considering the initial electron velocity as negligible, i.e., $v_F \approx 0$. The theoretical spectrum clearly displays the footprints of both, the CEP and the binary ridge, coming from the inner-shell and valence contributions, respectively. Calculated electron emission yields coincide with the experimental values for large electron velocities, but in the intermediate energy range, around the projection of the CEP, the theory underestimates the experiment. Similar behavior can be observed in Fig. 5 for the emission angle $\Omega_f = (\theta_e = 20°, \phi_e = 4.6°)$. Such discrepancies could be a consequence of the presence of other mechanisms not included in the theory.

Finally, in Fig. 6 we consider the ejection angle $\Omega_f = (\theta_e = 30°, \phi_e = 11.8°)$, which corresponds to the largest angles $\theta_e$ and $\phi_e$ studied in this work. Note that in all the cases considered, the core emission is extended over the whole electron energy range, tending slowly to zero for high electron velocities, while valence emission is only localized in the region determined by Eq. (18). At $\theta_e = 30°$, the theoretical and experimental spectra agree for low and intermediate

electron energies, where the inner-shell contribution is negligible. At high electron energies, where the core emission is the only possible binary mechanism, the theoretical curve runs slightly below the experimental data. This small difference may be caused by emission of energetic valence electrons as a consequence of multiple scattering processes [7], which are not contained in our formalism.

## V. CONCLUSIONS

We have presented theoretical and experimental results for the angle and energy distributions of electrons emitted during the grazing scattering of fast protons on an aluminum surface. From the theoretical point of view, we have put forward a consistent method to deal with the electron emission from metal surfaces. In the present model, partial contributions coming from inner-shell and valence-band electrons are calculated separately. The core emission is evaluated with a distorted-wave formalism, that we name FDW approximation. It incorporates approximately the effect of the induced surface potential on the atomic ionization. To calculate the emission from the valence band we employ the binary collisional formalism, using MSR model to represent the effective *P-e* interaction.

The relative importance of the contributions arising from the different sources of electrons of the metal has been analyzed as a function of the electron ejection angle. Theoretical electron emission yields are in reasonable agreement with the experiments for the different considered angles. In the forward direction, the inner-shell ionization is the dominant mechanism, the CEP being the most striking feature of the emission spectrum. When the ejection angle increases, valence emission begins to be relevant, and the signatures of the valence binary ridge appear in the electron distributions. And for very large angles, the valence contribution dominates at low and intermediate electron energies.

We have also investigated the action of the surface potential on the CEP by comparing the core emission probabilities calculated with and without including the surface interaction. We found that the induced field accelerates convoy electrons, and the influence of the surface interaction on ionized electrons diminishes rapidly as emission angle is separated from the forward direction. Another important effect, confirmed by the experiments, is that the broadens of CEP is well described by the enhancement factor (Jost function) given by a simple screening potential, which is used to represent the dynamic shielding of the projectile. In both, theoretical and experimental spectra, the CEP looks like a wide maximum instead of a sharp peak, characteristic of the Coulomb interactions.

## ACKNOWLEDGMENTS

The authors are very grateful to N.R. Arista for providing us data for the stopping of electrons. Financial support from the ANPCyT (PICTs 03-03579/06249/6325/4420), CONICET (PIP 0423), UBACyT (01-X044), ICTP-CLAF, and Fundación Antorchas (14116/86) are acknowledged and greatly valued.

[1] L. F. de Ferrariis and R. A. Baragiola, Phys. Rev. A **33**, 4449 (1986).
[2] K. Kimura, M. Tsuji, and M. Mannami, Phys. Rev. A **46**, 2618 (1992).
[3] J. Burgdörfer, in *Progress in Atomic and Molecular Physics*, edited by C. D. Lin (World Scientific, Singapore, 1993).
[4] E. A. Sánchez, O. Grizzi, M. L. Martiarena, and V. H. Ponce, Phys. Rev. Lett. **71**, 801 (1993).
[5] C. O. Reinhold, J. Burgdörfer, K. Kimura, and M. Mannami, Phys. Rev. Lett. **73**, 2508 (1994).
[6] M. L. Martiarena, E. A. Sánchez, O. Grizzi, and V. H. Ponce, Phys. Rev. A **53**, 895 (1992); Nucl. Instrum. Methods Phys. Res. B **90**, 300 (1994).
[7] C. O. Reinhold and J. Burgdörfer, Phys. Rev. A **55**, 450 (1997).
[8] G. R. Gómez, E. A. Sánchez, O. Grizzi, M. L. Martiarena, and V. H. Ponce, Nucl. Instrum. Methods Phys. Res. B **122**, 171 (1997).
[9] R. Minniti, S. B. Elston, C. O. Reinhold, J. Y. Lim, and J. Burgdörfer, Phys. Rev. A **57**, 2731 (1998).
[10] G. R. Gómez, O. Grizzi, E. A. Sánchez, and V. H. Ponce, Phys. Rev. B **58**, 7403 (1998).
[11] K. Kimura, S. Usui, and K. Nakajima, Phys. Rev. A **62**, 062902 (2000).
[12] M. S. Gravielle, Phys. Rev. A **62**, 062903 (2000).
[13] K. Kimura, S. Usui, K. Maeda, and K. Nakajima, Nucl. Instrum. Methods Phys. Res. B **193**, 661 (2002).
[14] J. E. Miraglia, Phys. Rev. A **50**, 2410 (1994).
[15] M. S. Gravielle and J. E. Miraglia, Phys. Rev. A **50**, 2425 (1994); **50**, 3202 (1994).
[16] M. S. Gravielle and J. E. Miraglia, Phys. Rev. A **67**, 042901 (2003).
[17] M. S. Gravielle and J. E. Miraglia, Phys. Rev. A **65**, 022901 (2002).
[18] S. M. Ritzau, R. A. Baragiola, and R. C. Monreal, Phys. Rev. B **59**, 15 506 (1999).
[19] E. A. Sánchez, J. E. Gayone, M. L. Martiarena, O. Grizzi, and R. A. Baragiola, Phys. Rev. B **61**, 14 209 (2000).
[20] G. Bocán and J. E. Miraglia, Phys. Rev. A **67**, 032902 (2003).
[21] D. M. Volkov, Z. Phys. **94**, 250 (1935).
[22] P. D. Fainstein, V. H. Ponce, and R. D. Rivarola, J. Phys. B **21**, 287 (1988).
[23] F. J. García de Abajo and P. M. Echenique, Phys. Rev. B **46**, 2663 (1992); **48**, 13 399 (1993).
[24] M. Alducin, R. Díez Muiño, and J. I. Juaristi, J. Electron Spectrosc. Relat. Phenom. **129**, 105 (2003).
[25] J. E. Miraglia and M. S. Gravielle, Phys. Rev. A **66**, 032901 (2002).
[26] N. R. Arista (private communication).
[27] M. R.C. McDowell and J. P. Coleman, *Introduction to the*

*Theory of Ion-Atom Collisions* (North-Holland, Amsterdam, 1970).
[28] E. Clementi and C. Roetti, At. Data Nucl. Data Tables **14**, 177 (1974).
[29] F. Salvat, J. M. Fernández-Varea, and M. Williamson, Jr., Comput. Phys. Commun. **90**, 51 (1995).
[30] M. S. Gravielle, Phys. Rev. A **58**, 4622 (1998).
[31] M. S. Gravielle, D. G. Arbó, and J. E. Miraglia, Nucl. Instrum. Methods Phys. Res. B **182**, 29 (2001).
[32] J. Lindhard and A. Winther, Mat. Fys. Medd. K. Dan. Vidensk. Selsk. **34**, 4 (1964).
[33] N. D. Mermin, Phys. Rev. B **1**, 2362 (1970).
[34] L. F. De Ferrariis, F. Tutzauer, E. A. Sánchez, and R. A. Baragiola, Nucl. Instrum. Methods Phys. Res. B **281**, 43 (1989).
[35] E. A. Sánchez, O. Grizzi, G. Nadal, G. Gómez, M. L. Martiarena, and V. H. Ponce, Nucl. Instrum. Methods Phys. Res. B **90**, 261 (1994).
[36] O. Grizzi, E. A. Sánchez, J. E. Gayone, L. Guillemot, V. A. Esaulov, and R. A. Baragiola, Surf. Sci. **260**, 71 (2000).
[37] N. R. Arista, Phys. Rev. A **49**, 1885 (1994).
[38] V. G. Molière, Z. Naturforsch. A **2**, 133 (1947).